



Published in final edited form as:

Science. 2025 January 24; 387(6732): 413–420. doi:10.1126/science.adr6896.

## Affinity maturation of antibody responses is mediated by differential plasma cell proliferation

Andrew J. MacLean<sup>1,\*</sup>, Lachlan P. Deimel<sup>1</sup>, Pengcheng Zhou<sup>1</sup>, Mohamed A. ElTanbouly<sup>1</sup>, Julia Merckenschlager<sup>1,†</sup>, Victor Ramos<sup>1</sup>, Gabriela S. Santos<sup>1</sup>, Thomas Hägglöf<sup>1</sup>, Christian T. Mayer<sup>2</sup>, Brianna Hernandez<sup>1</sup>, Anna Gazumyan<sup>1</sup>, Michel C. Nussenzweig<sup>1,3,\*</sup>

<sup>1</sup>Laboratory of Molecular Immunology, The Rockefeller University, New York, NY, 10065, USA

<sup>2</sup>Experimental Immunology Branch, Center for Cancer Research, National Cancer Institute, National Institutes of Health, Bethesda, MD 20892, USA

<sup>3</sup>Howard Hughes Medical Institute (HHMI), The Rockefeller University, New York, NY 10065, USA

### Abstract

Increased antibody affinity over time after vaccination, known as affinity maturation, is a prototypical feature of immune responses. Recent studies have shown that a diverse collection of B cells, producing antibodies with a wide spectrum of different affinities, are selected into the plasma cell (PC) pathway. How affinity-permissive selection enables PC affinity maturation remains unknown. We found that PC precursors (prePC) expressing high affinity antibodies received higher levels of T follicular helper (Tfh)-derived help and divided at higher rates than their lower affinity counterparts once they left the GC. Our findings indicate that differential cell division by selected prePCs accounts for how diverse precursors develop into a PC compartment that mediates serological affinity maturation.

### Main text:

Increasing antibody affinity over time after vaccination is a prototypical feature of humoral immune responses. Experiments in transgenic mice suggest that in the early germinal center (GC)-independent stages of the immune response, B cells expressing high affinity B cell receptors are preferentially selected into the PC compartment (1–3).

This article is subject to HHMI's Open Access to Publications policy. HHMI lab heads have previously granted a nonexclusive CC BY 4.0 license to the public and a sublicensable license to HHMI in their research articles. Pursuant to those licenses, the Author Accepted Manuscript (AAM) of this article can be made freely available under a CC BY 4.0 license immediately upon publication

\*Corresponding authors: nussen@rockefeller.edu, amaclean@rockefeller.edu.

†Present address: Department of Immunology, Harvard Medical School, Boston, MA 02115, USA

#### Author Contributions

A.J.M and M.C.N conceived the study, designed experiments, interpreted data and wrote the manuscript. A.J.M, L.P.D, P.Z and J.M. designed and performed experiments. V.R. and G.S.S performed bioinformatic data analysis. M.A.E. designed and generated the Blimp1-CreERT2 mouse strain. A.G., T.H., M.A.E., C.T.M. and B.H. designed and produced critical reagents. A.J.M, L.P.D., P.Z., J.M., V.R., G.S.S., T.H., M.A.E., C.T.M., B.H., A.G., and M.C.N contributed to editing the manuscript.

#### Competing interests

MCN is on the scientific advisory board of Celldex Therapeutics. All other authors declare that they have no competing interests.

Selection within the GC reaction itself is governed by Tfh that recruit B cells and control the degree of B cell clonal expansion (4). B cells expressing receptors that bind to and can capture antigen displayed on the surface of follicular dendritic cells in the light zone (LZ) process and present antigens to a limited number of Tfh, in exchange for help signals. Selected LZ B cells initiate a transcriptional program that enables them to move into the dark zone (DZ) where they undergo division and somatic mutation before returning to the LZ to test their newly mutated receptors in subsequent rounds of selection. The number of division cycles and the speed of cell division in the DZ is directly related to the strength of Tfh signals and governed by the level of *Myc* expression (5–7). Iterative cycles of DZ division and LZ selection produce GC B cells with increasing affinity for the immunogen over the course of an immune response. However, loss of affinity due to persistent somatic mutation and evolution of the Tfh compartment eventually leads to GC diversification and increasing inclusion of lower affinity B cells (8–12).

High affinity cells of GC origin become enriched in the antibody-secreting PC compartment over time after immunization (13–16). This observation, in conjunction with the known selection mechanisms within the GC, originally supported a model whereby high affinity cells preferentially undergo PC differentiation. In contrast to these findings, three recent independent studies have shown that in genetically intact animals, diverse collections of GC B cells develop into PC progenitors (8, 17, 18). In addition, these studies found little or no enrichment for high-affinity antibody expressing cells among the precursor population, prePCs (19, 20), in the GC (8, 17, 18). How this population of GC precursors that expresses antibodies with a broad range of affinities gives rise to a PC compartment dominated by cells producing high affinity antibodies is not understood.

## Results

### High-affinity cells are over-represented in PC compartment

To examine the relationship between GC B and PCs we tracked the two cell types using fate-mapping S1pr2-CreERT2 R26<sup>lsl-ZS<sup>Green</sup></sup> mice in which tamoxifen administration permanently labels GC cells and their subsequent products (21). Administration of tamoxifen to immunized mice confirmed that this reporter strain labels GC B cells and activated B cells, but not mature PCs (fig. S1A–C). Tamoxifen was administered 5 days after immunization with the model hapten antigen 4-hydroxy-3-nitrophenyl (NP) conjugated to the carrier protein ovalbumin (OVA; NP-OVA), and single cell sequencing was performed on labelled GC B and PCs isolated from the draining lymph node on day 14 (Fig. 1A,B). Uniform manifold approximation and projection (UMAP) integrating CITEseq data revealed distinct clusters of GC B and PCs characterized by Fas/CD86 and CD138 surface protein expression respectively (fig. S2).

Immunoglobulin sequence analysis showed expanded clones of cells that were further subdivided into nodes containing one or more cells expressing identical antibodies. The combined clonal trees consisted of 535 individual nodes with 1 to >100 members (Fig. 1C). Based on surface staining and gene expression profiles, nodes were divided into those consisting only of GC B cells, both GC B and PCs (“mixed nodes”), or only PCs. Nodes consisting of PCs only were the least abundant, representing <8% of the nodes (38/535

nodes, Fig. 1D). Most PCs were found within mixed nodes that were also larger than either GC- or PC-only nodes (Fig. 1E–G). IGHV1–72 antibody expression is associated with relatively high affinity NP binding (22). Notably, compared to GC nodes, nodes containing PCs were enriched for affinity enhancing mutations in IGHV1–72 (W33L/K59R/Y99G (22, 23); Fig. 1H). Furthermore, irrespective of node identity, PCs were enriched for affinity-enhancing mutations compared to contemporaneously labelled GC B cells ( $63 \pm 23\%$  PC vs  $42 \pm 11\%$  GC,  $p=0.02$ ; Fig. 1I). Thus, although prePC antibody affinity is indistinguishable from contemporaneous GC B cells (8, 17, 18), PCs are enriched for high affinity antibodies. Moreover, the presence of identical antibody sequences in large, expanded nodes containing GC and PCs suggests that the mechanisms that govern clonal expansion of the two cell types overlap.

### Differential expansion of high-affinity PCs

Two non-exclusive cellular processes could contribute to the observed enrichment of high-affinity PCs over GC B cells; differential cell death and/or division.

To determine whether cell death contributed to PC affinity maturation, we purified live and dying PCs from draining lymph nodes of NP-OVA-immunized mice using the Rosa26<sup>INDIA/INDIA</sup> apoptosis reporter mice (24). Ig sequence analysis revealed similar abundance of high affinity IGHV1–72 expressing cells in live and dying PC fractions (fig. S3A–D). In addition, most Ig sequences found among apoptotic PC clones were also present in the live fraction (fig. S3C). Thus, differential cell death did not appear to drive the accumulation of high affinity PCs over time.

To determine whether high affinity PCs have a proliferative advantage we tracked cell division using Vav<sup>tTa</sup> Col1A1-tetO-histone H2B<sup>mCherry</sup> reporter mice (H2B-mCherry) (25). Under steady state conditions, tTA is expressed in hematopoietic cells and induces high levels of the histone H2B-mCherry fusion protein expression. Administration of doxycycline represses histone H2B-mCherry synthesis, and therefore mCherry fluorescence dilutes in proportion to cell division (25). H2B-mCherry mice were immunized with NP-OVA and were administered doxycycline 10 days after immunization. PCs were isolated from draining lymph nodes 2 days later on the basis of their high or low levels of division (mCherry<sup>lo</sup> and mCherry<sup>hi</sup> PCs, respectively; Fig. 2A,B). mCherry<sup>lo</sup> PCs that had undergone greater levels of division showed reduced species richness and larger clonal families when compared to their non-dividing counterparts, indicating rapid clonal expansion in this population (Fig. 2C–E). Notably, there was an enrichment of PC expressing high-affinity IGHV1–72 among the more divided PCs ( $75.1 \pm 14\%$  mCherry<sup>lo</sup> vs  $37.1 \pm 12\%$  mCherry<sup>hi</sup>;  $p=0.0001$ ; Fig. 2F,G). At this early timepoint the W33L/K59R/Y99G affinity enhancing mutations were largely absent from both IGHV1–72<sup>+</sup> PCs populations, but there was a trend towards enrichment in the more divided mCherry<sup>lo</sup> group (Fig. 2H,  $p=0.08$ ). These findings were confirmed using Blimp1-CreERT2 R26<sup>lsl-ZSGreen</sup> mice, a reporter strain which selectively labels differentiated PCs (fig. S4A–B). Blimp1-CreERT2 R26<sup>lsl-ZSGreen</sup> mice were combined with H2B-mCherry mice to enable tamoxifen-mediated ZSG-labelling of a synchronized cohort of PCs which can be division-tracked by mCherry dilution. Isolation of mCherry<sup>Hi</sup> and mCherry<sup>Lo</sup> ZSG<sup>+</sup> PCs revealed that amongst mature PCs, the more

proliferative cells were enriched for NP bait binding, and expression of high-affinity Ig gene rearrangements (fig. S4C–H). These data indicated that higher affinity B cell receptor expression was associated with differential division at the mature PC stage.

To validate these findings using vaccine antigens, we immunized H2B-mCherry mice with either SARS-CoV2 receptor binding domain (RBD) or combined tetanus and diphtheria toxoid antigens (Tenivac<sup>®</sup>) and administered doxycycline on day 10 after vaccination. Antigen binding was used as a surrogate for higher affinity antigen binding cells (fig. S5A,B). Flow cytometric analysis revealed that RBD or tetanus and diphtheria toxoid binding cells were enriched and showed higher mean fluorescence among the divided mCherry<sup>lo</sup> compared to mCherry<sup>hi</sup> cells, even when normalized for surface Ig expression levels (fig. S5C–H). The combined data set indicated that high affinity plasma cells underwent greater levels of clonal expansion than lower affinity PCs irrespective of the composition of the administered immunogen or adjuvant formulation.

### PC selection outside of the GC

To examine the site of affinity-driven PC clonal expansion, S1pr2-CreERT2 R26<sup>lsl-ZSGreen</sup> mice were immunized with NP-OVA, treated with tamoxifen on day 8 and then given anti-CD40L or isotype control antibodies on day 10 and 12 after immunization. In this setting, tamoxifen will label GC products and anti-CD40L will terminate the GC reaction 2 days later, allowing a cohort of PCs generated between days 8–10 to be tracked. Draining lymph nodes were examined by confocal microscopy on day 16 after immunization (Fig. 3A,B, and fig. S6A).

Large GCs in which many of the cells were actively dividing (as determined by positive staining for Ki67) were observed in control mice that did not receive anti-CD40L. In addition, we found discrete clusters of dividing NP-binding PCs (marked by CD138<sup>+</sup>ZSG<sup>+</sup>Ki67<sup>+</sup>NP<sup>+</sup>) which were particularly abundant in the LN medulla. Anti-CD40L treatment aborted the GC reaction (Fig. 3A–B, and fig. S6A–B). In contrast, the clusters of proliferating NP-specific PCs persisted (Fig. 3A–B). Quantitation of medullary PC division by Ki67 staining revealed a higher proportion of dividing NP-binding than non-binding PCs. Moreover, this feature was retained upon anti-CD40L treatment and GC depletion (Fig. 3C–D). Thus, dividing antigen-specific PCs were observed in medullary foci outside of the anatomical confines of the GC, and these foci were maintained in the absence of active GCs during the observation period.

To determine whether the observed enrichment of high affinity PCs continued in a post-GC compartment, we isolated plasma cells from anti-CD40L treated S1pr2-CreERT2 R26<sup>lsl-ZSGreen</sup> mice. The mice also received the drug FTY720, to inhibit S1PR1-driven egress signals and to prevent PCs from leaving the node (26). Treatment with anti-CD40L effectively depleted draining lymph nodes of GCs and activated B cells within 2 days (Fig. 3A,B, and fig. S6A–D). Immunoglobulin sequence analysis on day 10 showed that 67% of labelled PCs were IGHV1–72<sup>+</sup>, and that by day 16 this increased to 83% under control conditions (p=0.037, Fig. 4A–E). Notably, the PC compartment was equally enriched for high affinity clones on day 16 in mice treated with anti-CD40L, under conditions that depleted GCs (Fig. 4C–E). In addition, the PC compartment in CD40L-treated mice

displayed the same characteristic reduction in species richness that was indicative of clonal expansion seen in control mice (Fig. 4B,F). Finally, labeled PCs obtained from anti-CD40L-treated mice displayed a reduced mutational load, suggesting that they were derived from GC precursors that exited the GC at a time when mutations were less abundant (Fig. 4G).

Serological affinity maturation is typified by a rapid increase in the affinity of circulating antibodies (27). We hypothesized that the continued preferential expansion of high affinity PCs after GC-depletion (Fig. 4A–G) would lead to measurable improvements of serum anti-NP affinity. To determine whether PCs in anti-CD40L treated mice continue to support affinity maturation after depletion of GC and activated B cells, we measured the serum antibody binding to bovine serum albumin derivatized with either 7 or 28 molecules of NP (Fig. 4H and fig. S6A–E). Control mice displayed a marked increase in NP<sub>7</sub>/NP<sub>28</sub> IgG binding between days 12 and 32 indicating a rapid increase in anti-NP affinity that was aborted by depleting PCs with TACI-Ig (Fig. 4I). Notably, and consistent with the above sequencing data, the serum antibody response continued to undergo affinity maturation for several weeks after anti-CD40L treatment (Fig. 4I,J).

We concluded that serological affinity maturation can proceed in the absence of continued output from the GC reaction, and it was suppressed by plasma cell depletion. These findings suggest that post-export from the germinal center, newly generated PCs undergo affinity-based expansion in a manner that contributes to increasing serum antibody affinity.

### PC division is proportional to the strength of T cell help

GC B cells in the LZ of the GC structure compete for limited help signals from T follicular helper (Tfh) cells, a process known as positive selection. The amount of help received by a B cell is directly proportional to the amount of antigen captured and presented by the B cell (25, 28). Positively selected GC B cells upregulate expression of the transcription factor *Myc* in proportion to the strength of T cell signals and migrate to the DZ where they undergo cycles of Tfh independent inertial cell division in proportion to the amount of *Myc* expression (5, 25, 29).

To determine whether a similar process regulated the relative amount of PC expansion, we delivered graded doses of the antigen ovalbumin (OVA) to ongoing GCs using chimeric anti-DEC205-OVA antibodies (28) (Fig. 5A). Protein antigens loaded onto anti-DEC205 are delivered to DEC205<sup>+</sup> GC B cells, supplying a B cell receptor-independent supply of antigen which can be processed and presented to Tfh cells (28). As expected, GC B cells expanded in direct proportion to the amount of antigen delivered (Fig. 5B,C). Antigen delivery by anti-DEC-205-OVA also produced a rapid increase in the frequency and numbers of prePCs (B220<sup>hi</sup> CD38<sup>−</sup> Fas<sup>+</sup> CD138<sup>+</sup>; Fig. 5B,D). To determine whether prePCs in the LZ of the GC also expressed *Myc* in proportion to antigen delivery by DEC-205, we purified these cells 24 hours after graded doses of anti-DEC-205-OVA injection. Consistent with their commitment to the plasma cell fate these cells displayed elevated levels of *Irf4*, a transcription factor which promotes PC differentiation, and lower expression levels of the antigen receptor signaling-induced factor *Nr4a1* than other LZ GC B (fig. S7A,B). Notably they showed increases in *Myc* that were directly proportional to the amount of antigen delivered (Fig. 5E). *Tfap4*, a transcription factor downstream of c-Myc, also showed a

similar induction pattern, although the expression of this factor plateaued at lower antigen concentrations (Fig. 5F). In addition, PrePC proliferation, as measured by Ki67 expression, was proportional to the amount of antigen supplied (fig. S7C,D).

To test whether Tfh help in the LZ could support continued PC expansion, anti-CD40L was administered 12 hours after anti-DEC-205-OVA. In this setting GC B cells acquired high levels of cognate antigen and interact with Tfh for ~12h, after which subsequent T cell help was inhibited by CD40L blockade as evidenced by GC collapse (Fig. 5G, Fig. 3A,B, and fig. S6A–B). Treatment with anti-CD40L 12h after anti-DEC205-OVA injection prevented further GC B cell expansion and blocked additional Ki67 expression in GC B including prePCs (Fig. 5H,I, and fig. S7E,F). In contrast, mature PCs continued to expand and divide in the days following anti-CD40L-treatment in direct proportion to the amount of antigen captured (Fig. 5J,K). The data indicated that after a short pulse of T cell help, developing prePCs upregulated *Myc* and underwent cycles of cell division in the absence of continued T cell signals.

Other signals are known to enhance the magnitude of the PC response (14). For example, PCs are highly sensitive to the levels of the cytokine IL-21 (30, 31), and IL-21- producing T cells have been reported to localize in foci outside of the B cell follicle (32). To test whether IL-21 could support the expansion of committed PCs, we fate-mapped PCs on day 8 using Blimp1-CreERT2 reporter mice and subsequently treated with anti-CD40L or anti-IL21R from days 10–12. PC division was assessed by Ki67 staining. As expected, analysis of ZSG-labelled PCs revealed that continued CD40L signals were not required to sustain PC proliferation (fig. S8A–C). In contrast, partial blockade of IL-21R led to reduced proliferation of mature ZSG<sup>+</sup> PCs, indicating that IL-21 supports the post-GC expansion of plasma cells (fig. S8B–C).

## Discussion

Current models of PC differentiation suggest that B cell receptor affinity is deterministic of cell fate (14, 15, 27). Our experiments indicated that while a heterogeneous collection of prePCs, including those expressing low affinity receptors, developed into PCs they subsequently underwent differential affinity dependent division. As a result, PCs expressing higher affinity antibodies contributed disproportionately to serum antibodies, promoting affinity maturation.

Antibody responses develop in two stages, a GC independent early phase during which B cells rapidly develop into dividing plasmablasts that produce relatively lower affinity antibodies and a second GC dependent phase that produces higher affinity antibodies responsible for serologic affinity maturation. In transgenic mice that carry high affinity antibodies, the early GC independent rapid burst of PC development and expansion is affinity dependent (1, 2). In contrast, under physiologic circumstances this early PC response produces primarily germline encoded antibodies with relatively lower affinity than those produced in GCs (15, 33, 34). In animals with a polyclonal B cell repertoire, GCs enable B cell clonal expansion and antibody hypermutation, both of which are essential for antibody



affinity maturation (27, 35, 36). Our experiments elucidated the mechanisms by which GC-dependent PC selection enables affinity maturation in polyclonal immune responses.

The GC LZ also contains prePCs that express IRF4, CD138, variable levels of *Myc*, and share many of the transcriptional features of LZ B cells selected for DZ re-entry (8, 14). Like DZ B cells, PC descendants of prePCs undergo rapid cell division in GC adjacent sites but they do not undergo additional somatic mutation and so retain antibody specificity (37). Our experiments show that the amount of clonal expansion by newly exported PCs was directly proportional to affinity and the strength of historic selection signals these cells received in the LZ, providing a mechanistic explanation for how PC selection is regulated in relation to affinity. Notably, our data is entirely consistent with the observation that the PC pool tends to be more clonal than contemporary GC B or pre-PCs from which they develop (8, 17). In addition to PCs in the LNs, long-lived PCs in the bone marrow are also enriched for high affinity antibody producing cells (38, 39). Our data suggests that this phenomenon is likely due to over-representation of high affinity PCs among dividing plasmablasts that subsequently seed the bone marrow.

In summary, post-GC PC clonal expansion in proportion to historical Tfh signals and *Myc* expression parallels *Myc*-regulated GC B cell clonal expansion, thereby enabling rapid affinity maturation. The proposed model does not preclude permissive selection of GC cells with diverse affinities into the PC compartment (8, 17, 18). Instead, our findings help resolve the apparent contradiction between affinity permissive selection into the PC compartment and rapid affinity maturation.

## Supplementary Material

Refer to Web version on PubMed Central for supplementary material.

## Acknowledgements

We thank T. Kurosaki for providing S1pr2-CreERT2 mice, T. Eisenreich for mouse colony management, K. Gordon for cell sorting, Anna Minh Newen for INDIA mice immunizations and all members of the Nussenzweig laboratory for helpful discussion.

## Funding

This work was supported in part by NIH grant 5R37 AI037526 and NIH Center for HIV/AIDS Vaccine Immunology and Immunogen Discovery (CHAVID) 1UM1AI144462-01 to M.C.N and the Stavros Niarchos Foundation Institute for Global Infectious Disease Research. J.M. is a Branco Weiss fellow. M.C.Nussenzweig is a Howard Hughes Medical Institute (HHMI) Investigator.

## Data and materials availability

All data needed to evaluate the conclusions in the paper are available in the main text and supplementary materials. Sequencing datasets have been deposited in NCBI's Gene Expression Omnibus, and are available through GEO accession number GSE282284. Reagents, including mouse strains, are available from A.J.M and M.C.N under a material transfer agreement with The Rockefeller University.

## References and notes

1. Paus D et al. , Antigen recognition strength regulates the choice between extrafollicular plasma cell and germinal center B cell differentiation. *J Exp Med* 203, 1081–1091 (2006). [PubMed: 16606676]
2. Chan TD et al. , Antigen affinity controls rapid T-dependent antibody production by driving the expansion rather than the differentiation or extrafollicular migration of early plasmablasts. *J Immunol* 183, 3139–3149 (2009). [PubMed: 19666691]
3. Phan TG et al. , High affinity germinal center B cells are actively selected into the plasma cell compartment. *J Exp Med* 203, 2419–2424 (2006). [PubMed: 17030950]
4. Crotty S, T Follicular Helper Cell Biology: A Decade of Discovery and Diseases. *Immunity* 50, 1132–1148 (2019). [PubMed: 31117010]
5. Finkin S, Hartweiger H, Oliveira TY, Kara EE, Nussenzweig MC, Protein Amounts of the MYC Transcription Factor Determine Germinal Center B Cell Division Capacity. *Immunity* 51, 324–336 e325 (2019). [PubMed: 31350178]
6. Dominguez-Sola D et al. , The proto-oncogene MYC is required for selection in the germinal center and cyclic reentry. *Nat Immunol* 13, 1083–1091 (2012). [PubMed: 23001145]
7. Calado DP et al. , The cell-cycle regulator c-Myc is essential for the formation and maintenance of germinal centers. *Nat Immunol* 13, 1092–1100 (2012). [PubMed: 23001146]
8. ElTanbouly MA et al. , Role of affinity in plasma cell development in the germinal center light zone. *J Exp Med* 221, (2024).
9. Hagglof T et al. , Continuous germinal center invasion contributes to the diversity of the immune response. *Cell* 186, 147–161 e115 (2023). [PubMed: 36565698]
10. de Carvalho RVH et al. , Clonal replacement sustains long-lived germinal centers primed by respiratory viruses. *Cell* 186, 131–146 e113 (2023). [PubMed: 36565697]
11. Merkenschlager J et al. , Dynamic regulation of T(FH) selection during the germinal centre reaction. *Nature* 591, 458–463 (2021). [PubMed: 33536617]
12. Merkenschlager J et al. , Continually recruited naive T cells contribute to the follicular helper and regulatory T cell pools in germinal centers. *Nat Commun* 14, 6944 (2023). [PubMed: 37907454]
13. Shih TA, Meffre E, Roederer M, Nussenzweig MC, Role of BCR affinity in T cell dependent antibody responses in vivo. *Nat Immunol* 3, 570–575 (2002). [PubMed: 12021782]
14. Ise W, Kurosaki T, Plasma cell differentiation during the germinal center reaction. *Immunol Rev* 288, 64–74 (2019). [PubMed: 30874351]
15. Nutt SL, Hodgkin PD, Tarlinton DM, Corcoran LM, The generation of antibody-secreting plasma cells. *Nat Rev Immunol* 15, 160–171 (2015). [PubMed: 25698678]
16. Radbruch A et al. , Competence and competition: the challenge of becoming a long-lived plasma cell. *Nat Rev Immunol* 6, 741–750 (2006). [PubMed: 16977339]
17. Sprumont A, Rodrigues A, McGowan SJ, Bannard C, Bannard O, Germinal centers output clonally diverse plasma cell populations expressing high- and low-affinity antibodies. *Cell*, (2023).
18. Sutton HJ et al. , Lack of affinity signature for germinal center cells that have initiated plasma cell differentiation. *Immunity*, (2024).
19. Ise W et al. , T Follicular Helper Cell-Germinal Center B Cell Interaction Strength Regulates Entry into Plasma Cell or Recycling Germinal Center Cell Fate. *Immunity* 48, 702–715 e704 (2018). [PubMed: 29669250]
20. Krautler NJ et al. , Differentiation of germinal center B cells into plasma cells is initiated by high-affinity antigen and completed by Tfh cells. *J Exp Med* 214, 1259–1267 (2017). [PubMed: 28363897]
21. Shinnakasu R et al. , Regulated selection of germinal-center cells into the memory B cell compartment. *Nat Immunol* 17, 861–869 (2016). [PubMed: 27158841]
22. Allen D, Simon T, Sablitzky F, Rajewsky K, Cumano A, Antibody engineering for the analysis of affinity maturation of an anti-hapten response. *EMBO J* 7, 1995–2001 (1988). [PubMed: 3138111]
23. Furukawa K, Akasako-Furukawa A, Shirai H, Nakamura H, Azuma T, Junctional amino acids determine the maturation pathway of an antibody. *Immunity* 11, 329–338 (1999). [PubMed: 10514011]



24. Mayer CT et al. , The microanatomic segregation of selection by apoptosis in the germinal center. *Science* 358, (2017).
25. Gitlin AD, Shulman Z, Nussenzweig MC, Clonal selection in the germinal centre by regulated proliferation and hypermutation. *Nature* 509, 637–640 (2014). [PubMed: 24805232]
26. Kabashima K et al. , Plasma cell S1P1 expression determines secondary lymphoid organ retention versus bone marrow tropism. *J Exp Med* 203, 2683–2690 (2006). [PubMed: 17101733]
27. Victora GD, Nussenzweig MC, Germinal Centers. *Annu Rev Immunol* 40, 413–442 (2022). [PubMed: 35113731]
28. Victora GD et al. , Germinal center dynamics revealed by multiphoton microscopy with a photoactivatable fluorescent reporter. *Cell* 143, 592–605 (2010). [PubMed: 21074050]
29. Pae J et al. , Cyclin D3 drives inertial cell cycling in dark zone germinal center B cells. *J Exp Med* 218, (2021).
30. Chen Z et al. , Heparan sulfate regulates IL-21 bioavailability and signal strength that control germinal center B cell selection and differentiation. *Sci Immunol* 8, eadd1728 (2023). [PubMed: 36800411]
31. Ozaki K et al. , Regulation of B cell differentiation and plasma cell generation by IL-21, a novel inducer of Blimp-1 and Bcl-6. *J Immunol* 173, 5361–5371 (2004). [PubMed: 15494482]
32. Odegard JM et al. , ICOS-dependent extrafollicular helper T cells elicit IgG production via IL-21 in systemic autoimmunity. *J Exp Med* 205, 2873–2886 (2008). [PubMed: 18981236]
33. MacLennan IC et al. , Extrafollicular antibody responses. *Immunol Rev* 194, 8–18 (2003). [PubMed: 12846803]
34. Cyster JG, Allen CDC, B Cell Responses: Cell Interaction Dynamics and Decisions. *Cell* 177, 524–540 (2019). [PubMed: 31002794]
35. De Silva NS, Klein U, Dynamics of B cells in germinal centres. *Nat Rev Immunol* 15, 137–148 (2015). [PubMed: 25656706]
36. Jacob J, Kelsoe G, Rajewsky K, Weiss U, Intracloal generation of antibody mutants in germinal centres. *Nature* 354, 389–392 (1991). [PubMed: 1956400]
37. Zhang Y et al. , Plasma cell output from germinal centers is regulated by signals from Tfh and stromal cells. *J Exp Med* 215, 1227–1243 (2018). [PubMed: 29549115]
38. Robinson MJ et al. , Long-lived plasma cells accumulate in the bone marrow at a constant rate from early in an immune response. *Sci Immunol* 7, eabm8389 (2022). [PubMed: 36306370]
39. Takahashi Y, Dutta PR, Cerasoli DM, Kelsoe G, In situ studies of the primary immune response to (4-hydroxy-3-nitrophenyl)acetyl. V. Affinity maturation develops in two stages of clonal selection. *J Exp Med* 187, 885–895 (1998). [PubMed: 9500791]
40. Schaefer-Babajew D et al. , Antibody feedback regulates immune memory after SARS-CoV-2 mRNA vaccination. *Nature* 613, 735–742 (2023). [PubMed: 36473496]
41. Benson MJ et al. , Cutting edge: the dependence of plasma cells and independence of memory B cells on BAFF and APRIL. *J Immunol* 180, 3655–3659 (2008). [PubMed: 18322170]
42. Pasqual G, Angelini A, Victora GD, Triggering positive selection of germinal center B cells by antigen targeting to DEC-205. *Methods Mol Biol* 1291, 125–134 (2015). [PubMed: 25836306]
43. Viant C, Escolano A, Chen ST, Nussenzweig MC, Sequencing, cloning, and antigen binding analysis of monoclonal antibodies isolated from single mouse B cells. *STAR Protoc* 2, 100389 (2021). [PubMed: 33778783]
44. Cho A et al. , Anti-SARS-CoV-2 receptor-binding domain antibody evolution after mRNA vaccination. *Nature* 600, 517–522 (2021). [PubMed: 34619745]
45. Gaebler C et al. , Evolution of antibody immunity to SARS-CoV-2. *Nature* 591, 639–644 (2021). [PubMed: 33461210]
46. Wang Z et al. , Naturally enhanced neutralizing breadth against SARS-CoV-2 one year after infection. *Nature* 595, 426–431 (2021). [PubMed: 34126625]
47. MacLean AJ et al. , Secondary influenza challenge triggers resident memory B cell migration and rapid relocation to boost antibody secretion at infected sites. *Immunity* 55, 718–733 e718 (2022). [PubMed: 35349789]

48. Lefranc MP, IMGT, the International ImMunoGeneTics Information System. Cold Spring Harb Protoc 2011, 595–603 (2011). [PubMed: 21632786]
49. Katoh K, Misawa K, Kuma K, Miyata T, MAFFT: a novel method for rapid multiple sequence alignment based on fast Fourier transform. Nucleic Acids Res 30, 3059–3066 (2002). [PubMed: 12136088]
50. DeWitt WS 3rd, Mesin L, Victora GD, Minin VN, Matsen F. A. t., Using Genotype Abundance to Improve Phylogenetic Inference. Mol Biol Evol 35, 1253–1265 (2018). [PubMed: 29474671]

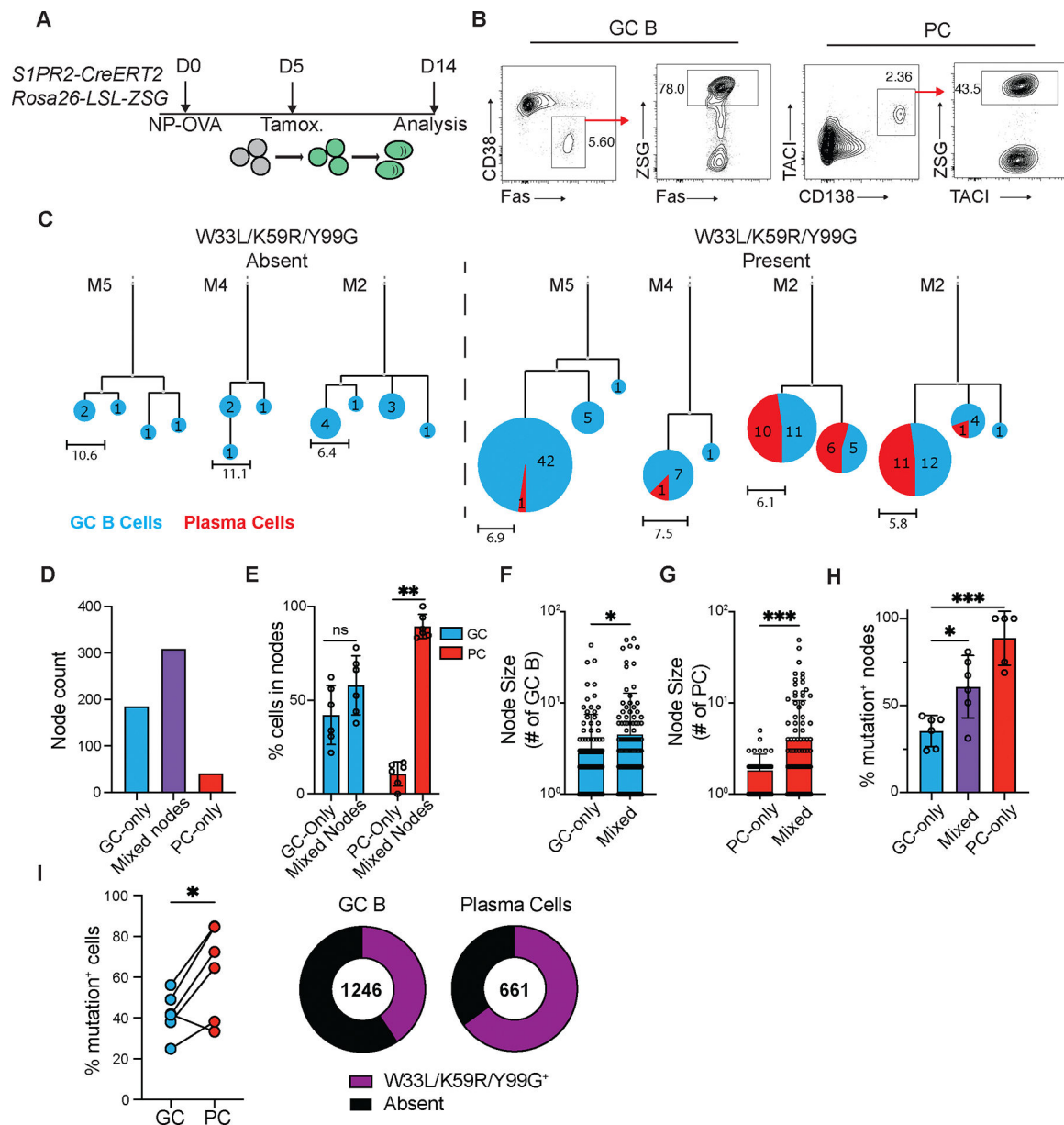


**Fig 1. High affinity antibody producing PCs are over-represented relative to contemporaneous GC B cells.**

(A) Experimental layout for (B-H). (B), Representative flow cytometry plots showing strategy for isolating popliteal LN (pLN) GC B cells (Pre-gated on live, TACI<sup>-</sup> CD138<sup>-</sup> B220<sup>+</sup>; CD38<sup>+</sup> Fas<sup>+</sup> ZSG<sup>+</sup>) and PCs (Pre-gated on live; CD138<sup>+</sup> TACI<sup>+</sup> ZSG<sup>+</sup>). Full gating strategy is displayed in fig. S2A. (C) Representative IgH+IgL sequence-based phylogenetic trees highlighting GC B cell (blue) and PC (red) distribution. Expanded clones containing (right) or not containing (left) affinity-enhancing mutations. Each circle represents one node of cells with identical sequences. Scale represents mutational distance observed between related sequences. (D) Total numbers of GC-only, PC-only or mixed nodes analyzed. (E) Frequency of GC B (blue bars) or PCs (red bars) found within mixed or single cell-type nodes. Each point represents one animal. (F-G) Node size; number of individual GC B

cells (**F**) or PCs (**G**) in either uniform or mixed nodes. (**H**) Frequency of nodes with affinity-enhancing mutations. Each point represents one mouse, summarizing 51–176 nodes per mouse. (**I**) Frequency of affinity-enhancing mutations within total GC B cells and PCs. Left, summary, each pair of connected points represents GC B cells and PCs isolated from one animal. Right, quantitation of total cells. Numbers in center represent total number of sequences analyzed. \*  $p < 0.05$ , \*\*\*  $p < 0.0005$ . (**F,G**) ANOVA; (**H**) mixed effects analysis; (**I**) paired two-tailed Student's t-test. Data are pooled from two independent experiments,  $n=6$ .

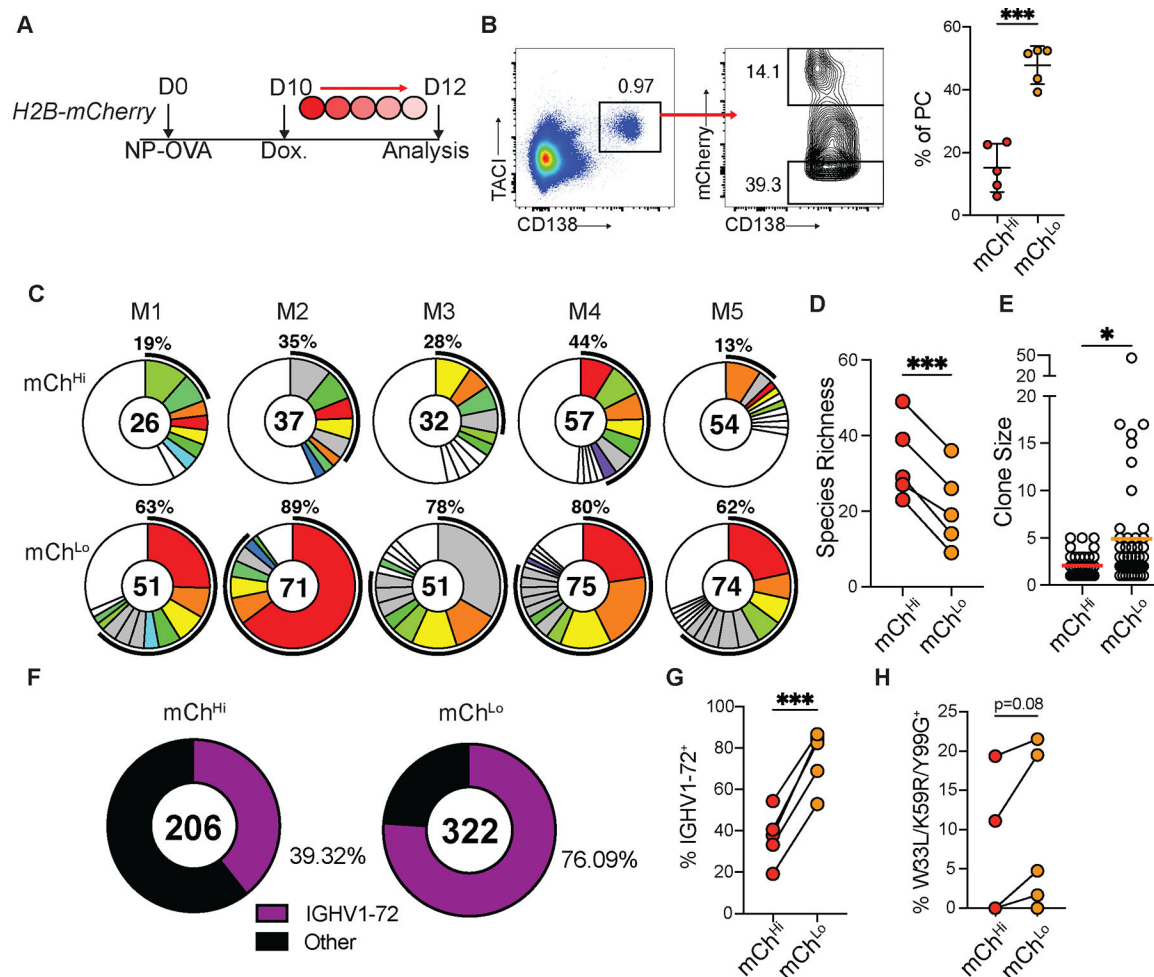


**Fig 2. High affinity antibody producing PCs are more proliferative.**

(A) Experimental layout for (B-F). (B) Left, flow cytometry profile showing TACI<sup>+</sup>CD138<sup>+</sup> PCs and gating for mCh<sup>hi</sup> and mCh<sup>lo</sup> cells from pLNs. Right, mCh<sup>lo</sup> and mCh<sup>hi</sup> PC frequency. Each point represents one mouse. Graphs display mean±SD. (C) Clonal distribution of paired Ig sequences (IgH+IgK/IgL) among mCh<sup>hi</sup> and mCh<sup>lo</sup> PCs isolated from each mouse. Colored segments represent expanded clones and singlets are represented by white segments. The number in the center represents the number of sequences analyzed per population. The outer segment annotation denotes the percentage of cells that are members of expanded clones. (D), Chao1 species richness quantification. Each pair of points represents one mouse. (E) Clone size. Each point represents one clone. (F) Frequency of mCh<sup>hi</sup> or mCh<sup>lo</sup> PCs bearing high-affinity IGHV1-72 BCRs. Number in center represents total number of sequences. (G) Summary of (F) each pair of points represents one mouse. (H) Frequency of high affinity mutation containing sequences among IGHV1-72<sup>+</sup> expressing mCh<sup>hi</sup> or mCh<sup>lo</sup> PCs. \* p<0.05, \*\*\* p<0.0005. (B,D,G,H) paired two-tailed Student's t-test; (E) unpaired Student's t-test. Data are pooled from 2 independent experiments, n=5.

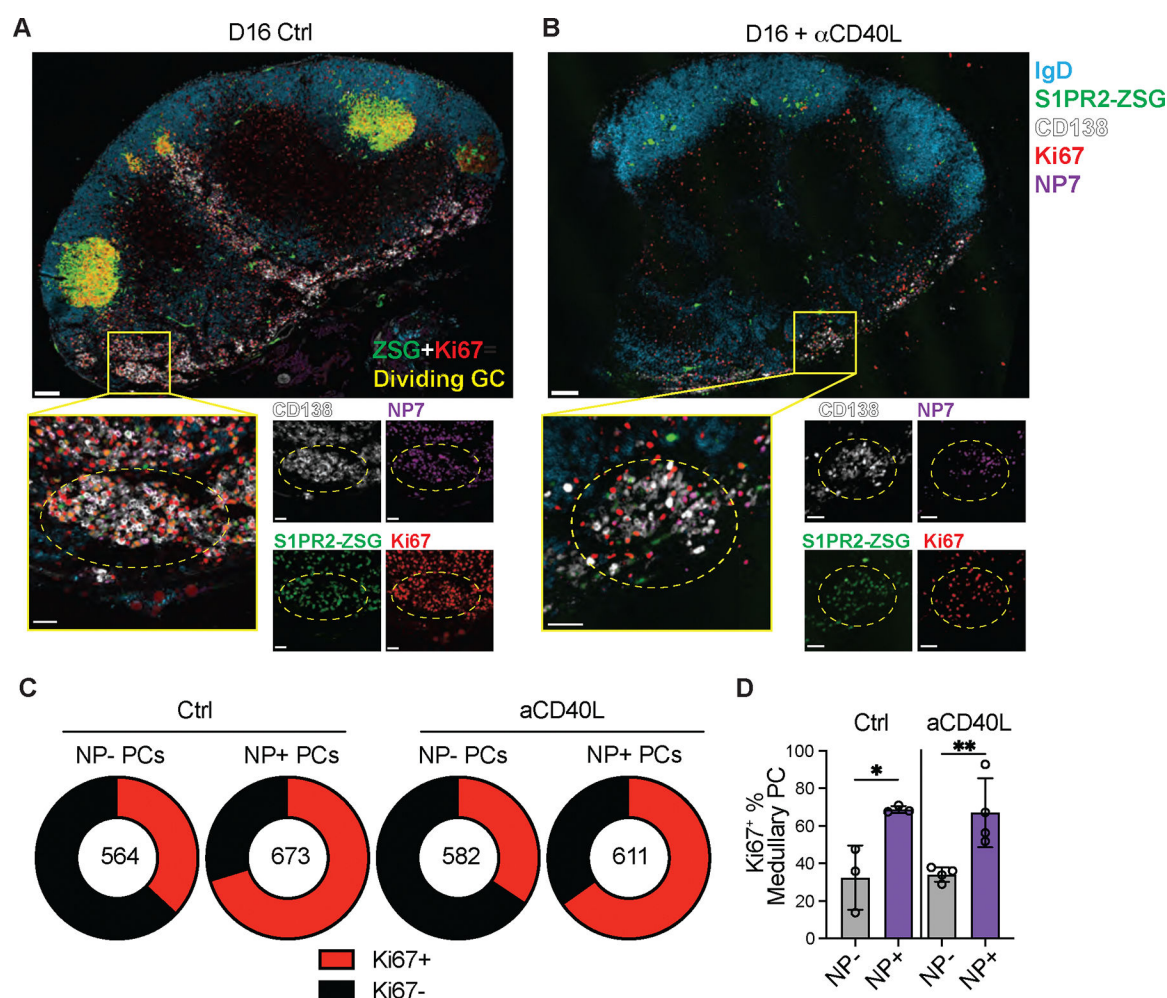


**Fig 3. Clonal evolution of the PC repertoire.**

(A-B), Confocal microscopy images of pLNs isolated from S1pr2-CreERT2 R26<sup>lsl-ZSGreen</sup> mice immunized with NP-OVA, treated with tamoxifen on D8 and anti-CD40L or isotype control on D10 and D12. Large tiles show overview of pLN architecture. Inset boxes show individual clusters of dividing Ki67<sup>+</sup> NP<sup>+</sup> PCs that are highlighted by dashed circles. Individual channels are shown beside merged images. In large tiles, scale bar=100 $\mu$ m. In inset boxes, scale bar=30 $\mu$ m. (C) Quantitation of fraction of medullary PCs which are Ki67<sup>+</sup> amongst NP<sup>+</sup> and NP<sup>-</sup> populations, as quantified from confocal images as in (A). The number in the center represents the number of cells analyzed per population. (D) Summary of (C); each point represents one mouse. Graph displays mean $\pm$ SD. \*p<0.05, \*\*p<0.005; ordinary one-way ANOVA. Data are representative of three experiments, n=3-4 per group.



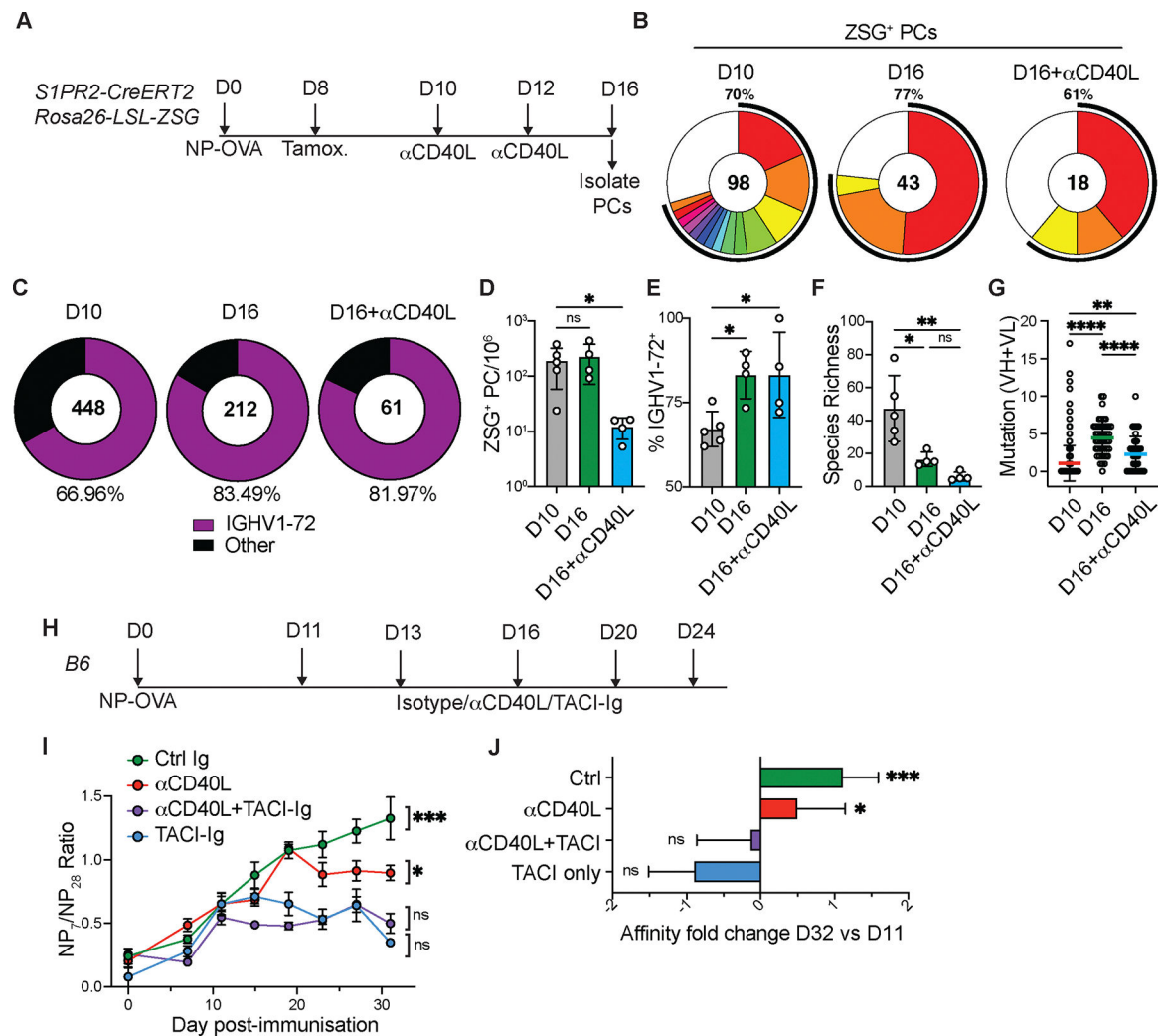


**Fig 4. Serological affinity maturation.**

(A) Experimental layout for (B-G). (B) Clonal distribution of paired Ig sequences from representative mice. Colored segments represent expanded clones and singlets are represented by white segments. The number in the center represents the number of sequences analyzed per population. The outer segment annotation denotes the percentage of cells that are members of expanded clones. (C) Frequency of ZSG<sup>+</sup> PCs expressing IGHV1-72. The number in the center represents the number of sequences analyzed. (D) Number of ZSG<sup>+</sup> PCs in each experimental group. (E) Summary of IGHV1-72 frequency presented in (C). (F) Chao1 species richness. In D-F, each point represents one mouse, n=4–5 per condition. (G) Number of VH+VL mutations in paired Ig sequences. Each point represents one cell. (H), Experimental layout for (I-J). (I) Ratio of NP<sub>7</sub>/NP<sub>28</sub>-binding IgG in serum measured by ELISA. (J) Fold change in affinity (NP<sub>7</sub>/NP<sub>28</sub> ratio) at D32 vs D11. Data are presented as mean±SD. Data are representative of two experiments, n=5–10 per group. \* p<0.05, \*\* p<0.005, \*\*\*\* p<0.0001. (D-F) ordinary one-way ANOVA; (G) Kruskal-Wallis test. (I-J), mixed effects analysis. For full statistical comparisons see Supplementary Fig.4E.

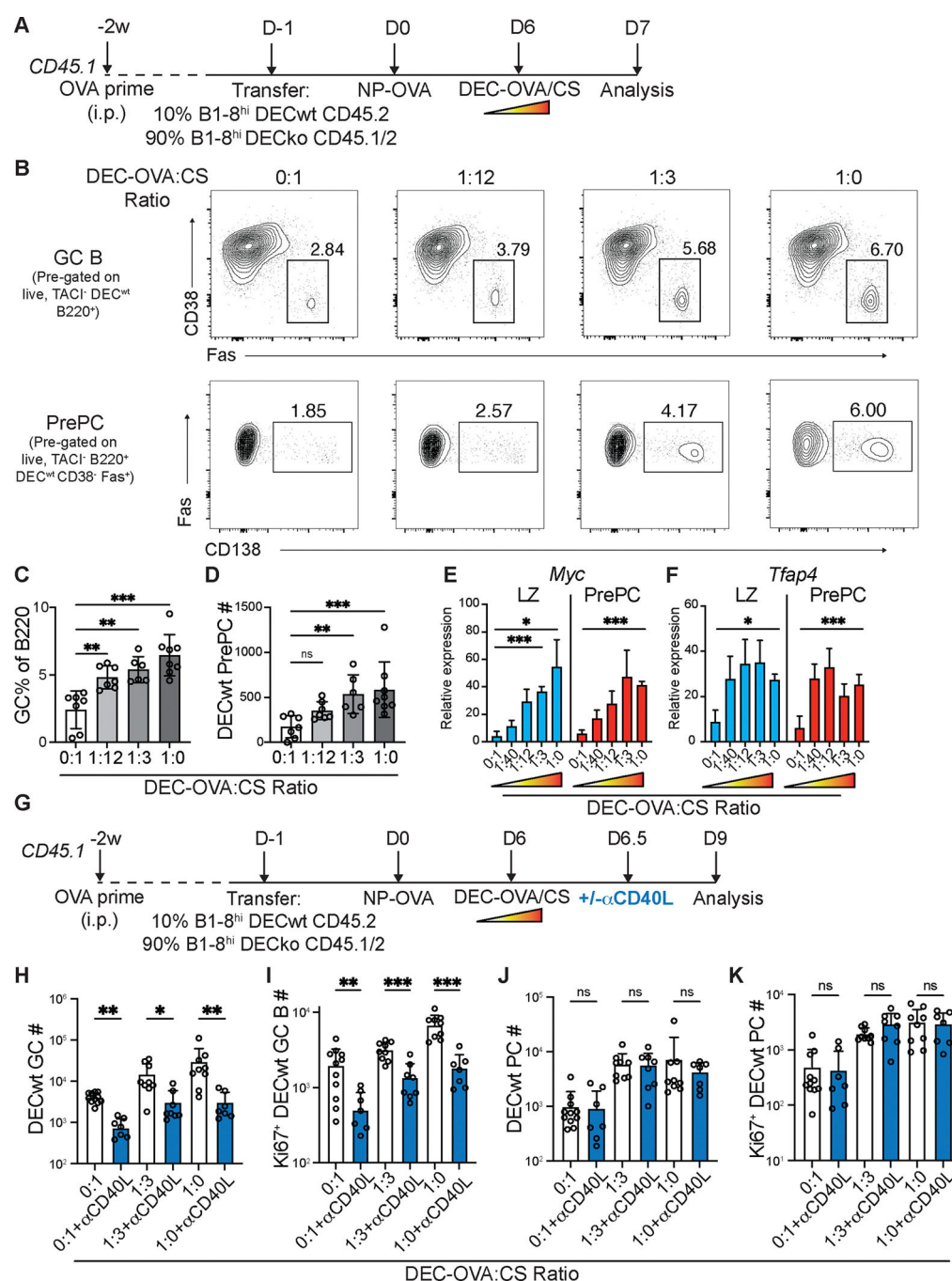


**Fig 5. PC proliferation is proportional to signal strength.**

(A) Experimental outline for (A-F). (B) Representative flow cytometry plots showing GC B cells (B220<sup>+</sup>CD38<sup>+</sup>Fas<sup>+</sup>, top) and prePCs (B220<sup>+</sup>CD38<sup>+</sup>Fas<sup>+</sup>CD138<sup>+</sup>, bottom), after treatment with different ratios of anti-DEC-OVA:CS. (C-D) Quantitation of DEC<sup>wt</sup> GC B cells (C) and prePCs (D) 24h after anti-DEC treatment. (E-F) qPCR of sorted DEC<sup>wt</sup> GC LZ (CD86<sup>+</sup>CXCR4<sup>+</sup> GC B) and prePC (as above) showing GAPDH-normalized relative expression for *Myc* (E) and *Tfap4* (F). Data in (A-D) and (E-F) are representative of 3 independent experiments, n=6-8 per group. (G) Experimental outline for (H-K). (H-

**I)** Quantitation of DEC<sup>WT</sup> GC B cells (**H**) and Ki67<sup>+</sup> DEC<sup>WT</sup> GC B cells (**I**). (**J-K**) Quantitation of DEC<sup>WT</sup> PCs (**J**) and Ki67<sup>+</sup> DEC<sup>WT</sup> PCs (**K**). Data are presented as mean $\pm$ SD. Each point in C,D, H-K represents one mouse. Data in (**H-K**) are representative of 4 independent experiments. \* p<0.05, \*\* p<0.005. (C) ANOVA; (**D, H-K**) Kruskal-Wallis test.